The Npc2Gt(LST105)BygNya mouse signifies pathological changes comparable to human Niemann-Pick type C2 disease

Rasmussen, Charlotte Laurfelt Munch; Thomsen, Louiza Bohn; Heegaard, Christian Würtz; Moos, Torben; Burkhart, Annette

Published in:
Molecular and Cellular Neuroscience

DOI (link to publication from Publisher):
10.1016/j.mcn.2023.103880

Publication date:
2023

Document Version
Publisher's PDF, also known as Version of record

Molecular and Cellular Neuroscience 126 (2023) 103880

Contents lists available at ScienceDirect

Molecular and Cellular Neuroscience

journal homepage: www.elsevier.com/locate/ymcne

The *Npc2*$^{Gt(LST105)BygNya}$ mouse signifies pathological changes comparable to human Niemann-Pick type C2 disease

Charlotte Laurfelt Munch Rasmussen [a], Louiza Bohn Thomsen [a], Christian Würtz Heegaard [b], Torben Moos [a], Annette Burkhart [a,*]

[a] Neurobiology Research and Drug Delivery, Department of Health Science and Technology, Aalborg University, Denmark
[b] Department of Molecular Biology and Genetics, Aarhus University, Aarhus, Denmark

ARTICLE INFO

Keywords:
Niemann-Pick type C2 disease
NPC2
Mouse models
Neurodegeneration
Cerebellar Purkinje cell

ABSTRACT

Introduction: Niemann-Pick type C2 disease (NP-C2) is a fatal neurovisceral disorder caused by defects in the lysosomal cholesterol transporter protein NPC2. Consequently, cholesterol and other lipids accumulate within the lysosomes, causing a heterogeneous spectrum of clinical manifestations. Murine models are essential for increasing the understanding of the complex pathology of NP-C2. This study, therefore, aims to describe the neurovisceral pathology in the NPC2-deficient mouse model to evaluate its correlation to human NP-C2.
Methods: *Npc2*−/− mice holding the LST105 mutation were used in the present study (*Npc2*$^{Gt(LST105)BygNya}$). Body and organ weight and histopathological evaluations were carried out in six and 12-week-old *Npc2*−/− mice, with a special emphasis on neuropathology. The Purkinje cell (PC) marker calbindin, the astrocytic marker GFAP, and the microglia marker IBA1 were included to assess PC degeneration and neuroinflammation, respectively. In addition, the pathology of the liver, lungs, and spleen was assessed using hematoxylin and eosin staining.
Results: Six weeks old pre-symptomatic *Npc2*−/− mice showed splenomegaly and obvious neuropathological changes, especially in the cerebellum, where initial PC loss and neuroinflammation were evident. The *Npc2*−/− mice developed neurological symptoms at eight weeks of age, severely progressing until the end-stage of the disease at 12 weeks. At the end-stage of the disease, *Npc2*−/− mice were characterized by growth retardation, tremor, cerebellar ataxia, splenomegaly, foam cell accumulation in the lungs, liver, and spleen, brain atrophy, pronounced PC degeneration, and severe neuroinflammation.
Conclusion: The *Npc2*$^{Gt(LST105)BygNya}$ mouse model resembles the pathology seen in NP-C2 patients and denotes a valuable model for increasing the understanding of the complex disease manifestation and is relevant for testing the efficacies of new treatment strategies.

1. Introduction

Niemann-Pick type C disease (NP-C) is an autosomal recessive lysosomal storage disease caused by a deficiency in either the intracellular cholesterol transporter proteins NPC1 or NPC2 (Wiweger et al., 2021). The incidence of NP-C is 1:100,000 live births, with the majority of cases caused by NPC1 deficiency (95 %), whereas NPC2 deficiency accounts for the remaining 5 % (Vanier, 2010). NPC1 is a large multidomain transmembrane protein located in the lysosomes, whereas NPC2 is a soluble sterol-binding protein targeted to the lysosomes by binding the mannose-6-phosphate receptor. The two proteins are believed to act in tandem mediating the efflux of free cholesterol and other lipids (e.g., gangliosides) from the *endo*-lysosomal compartment to other cellular compartments (e.g., endoplasmatic reticulum, trans-Golgi network, and plasma membrane) (Zhou et al., 2011; Li et al., 2016; Berzina et al., 2018). Mutations in the ubiquitously expressed *Npc1* or *Npc2* gene can lead to the loss of function or reduced activity of the gene products consequently resulting in an accumulation of cholesterol within the

Abbreviations: GFAP, Glial fibrillary acidic protein; IBA1, Ionized calcium-binding adaptor molecule 1; NP-C, Niemann-Pick type C disease; NP-C1, Niemann-Pick type C1 disease; NP-C2, Niemann-Pick type C2 disease; NPC1, Niemann-Pick C1 protein; NPC2, Niemann-Pick C2 protein; PC, Cerebellar Purkinje cell; PBS, Phosphate-buffered saline; PPBS, Potassium-containing phosphate-buffered saline; WT, Wild-type..

* Corresponding author at: Neurobiology Research and Drug Delivery, Department of Health Science and Technology, Fredrik Bajers Vej 3B, Room 2.205, Aalborg University, DK-9220 Aalborg East, Denmark.
E-mail address: abl@hst.aau.dk (A. Burkhart).

https://doi.org/10.1016/j.mcn.2023.103880
Received 17 March 2023; Received in revised form 10 July 2023; Accepted 11 July 2023
Available online 16 July 2023

lysosomes (Nielsen et al., 2011; Yañez et al., 2020). Therefore, the age of onset and clinical presentation is variable and includes a diverse range of visceral manifestations such as hepatosplenomegaly with liver dysfunction, pulmonary failure, and neurological symptoms such as cerebellar ataxia, dysphagia, dysarthria, and dementia. Progressive neurodegeneration results in a fatal outcome of the disease, and most patients die before the age of 30 years (Wiweger et al., 2021; Vanier, 2010; Liu et al., 2008). While several mouse models have been established to study NP-C1, only a few murine models are available for NP-C2. Even though the pathological hallmarks are indistinguishable between the spontaneous NP-C1 (*Npc1*^{nih}) mouse model and the induced NP-C2 mouse models, there are some discrepancies, e.g., when it comes to disease progression. The *Npc1*^{nih}-null mouse model is more progressive, leading to earlier death (9–11 weeks of age) compared to the hypomorphic NP-C2 mouse models (12–18 weeks of age), depending on background strain (Nielsen et al., 2011; Dixit et al., 2011; Sleat et al., 2004; Loftus et al., 1997).

Two transgenic hypomorphic NP-C2 mouse models are described in the literature, the *Npc2*^{tm1Plob} and the *Npc2*$^{Gt(LST105)BygNya}$, established by targeted mutation or the gene trap approach, respectively. While the *Npc2*^{tm1Plob} has been more widely used (Dixit et al., 2011; Sleat et al., 2004; Markmann et al., 2018; Roszell et al., 2013; Schrantz et al., 2007; Busso et al., 2010; Ong et al., 2004), only limited data are available for the *Npc2*$^{Gt(LST105)BygNya}$ mouse model (Nielsen et al., 2011; Schrantz et al., 2007).

Therefore, this study aimed to characterize the *Npc2*$^{Gt(LST105)BygNya}$ mouse model established on a BALB/c background with a primary focus on the pathological changes caused by NPC2 deficiency. Furthermore, a group of six-week-old mice was included to evaluate the degree of pathology before obvious symptoms are present, thereby evaluating the disease progression from six to 12 weeks of age. Finally, the pathological findings will be compared to the hallmarks of NP-C in humans to assess the translational value of this specific NP-C2 mouse model.

2. Materials and methods

2.1. Animals

The 129P2/OlaHsd-*Npc2*$^{Gt(LST105)BygNya}$ mouse strain maintained on a BALB/c background (Nielsen et al., 2011) was rederived using in vitro fertilization with sperm collected from gene carrier mice (*Npc2*+/−) (Nielsen et al., 2011) and embryos from BALB/cJRj mice (Janvier Labs). The mice were housed with up to five mice per cage (GM500 IVC, Techniplast) under standard conditions (12 h light/dark cycle at 20–24 °C and 55 ± 10 % humidity, and ad libitum access to food (Altromin 1324, Brogaarden) and water) in a specific pathogen-free facility. Environmental enrichment included Tapvei bedding material, sizzle nesting material, aspen bricks, peanuts, tunnels, and biodegradable cardboard houses. The cages were changed weekly. The mice were inspected daily by an animal caretaker. The animal study and breeding of *Npc2*-/- mice was approved by the Animal Experiments Inspectorate under the Ministry of Food, Agriculture, and Fisheries of Denmark (License no. 2018-15-0201-01467 and 2019-15-0202-00056).

2.2. Genotyping by qPCR

DNA was extracted from ear punches using the Quick-DNA mini prep plus kit (Zymo Research #D4068) between postnatal days 10 and 14. The offspring were genotyped using qPCR with the following DNA primer pairs: *Npc2* mutant (forward primer 5′-CCA GGC AGC ACG GAT GTC-3′ and reverse primer 5′-GCC AGG GTT TTC CCA GTC A-3′) and *Npc2* wild-type (forward primer 5′-TGT GGC TCA GTG GCT TAG G-3′ and reverse primer 5′-CCA GGA AGG GAT TTC ACA CA-3′) (Nielsen et al., 2011), and Maxima SYBR Green Master Mix, with ROX as a reference (Thermo Fisher Scientific, #K0223). The PCR conditions consisted of an initial denaturation step of 95 °C for 10 min followed by 40 cycles of denaturation at 95 °C for 15 s, annealing at 60 °C for 30 s, and extension at 72 °C for 30 s. Furthermore, a melt curve analysis was performed at 60 °C to 95 °C with 0.05 °C/s. Examples of genotyping data are provided in Fig. S1.

2.3. Breeding information

The breeding of NPC2-deficient mice (*Npc2*−/−) and wild-type (WT) littermates (*Npc2*+/+) was generated from the mating of heterozygous (*Npc2*+/−) mice. No backcrossing was performed after the rederivation. Continuous trio breeding was used for the breeding program, where one adult male was housed together with two adult females. Each experimental unit is therefore defined as a breeding cage when evaluating breeding data. Eight trio-breeding cages were used in the present study. The mice used for breeding were housed in GR900 IVC cages (Techniplast) and provided with Altromin 1318 diet ad libitum. During the lactation period, the diet was supplemented with peanuts. For each breeding cage, the following parameters were evaluated; the number of litters, litter size at birth (pups were counted between birth and two days), and interlitter interval (the number of days between births of consecutive litters). The litter size and body weight at weaning were also evaluated. The offspring were weaned after 21 days; 22 mice were included in the study (see Table 1 for the different experimental groups).

2.4. Euthanasia and tissue collection

Npc2−/− mice were euthanized either at six weeks of age before symptom development or at 12 weeks of age, before the end-stage of the disease, determined by severe tremor, ataxia, and/or weight loss of 20 % compared to healthy *Npc2*+/+ mice of identical age and sex. WT mice were also euthanized at 6 or 12 weeks of age and included as controls. The mice were deeply anesthetized by inhaling isoflurane (5 %, 1 L O_2/min) and were euthanized by exsanguination by perfusing with phosphate-buffered saline (PBS). The organs of interest (brain, lungs, liver, and spleen) were weighed and collected for histological and immunohistochemical examination and post-fixated in 4 % paraformaldehyde (PFA) overnight (4 °C). On the following day, the organs were washed in potassium-containing PBS (PPBS) and stored in 0.03 % sodium azide until further processing.

2.5. Histological and immunohistochemical staining

Brains were cut into coronal sections (40 μm) using a cryostat and collected free-floating in PPBS in a sequential series of six. The brain sections were incubated free-floating in a blocking buffer containing 3 % porcine serum with 0.3 % Triton X-100 diluted in 0.1 M PPBS for 30 min at room temperature. Afterward, the sections were incubated with the following primary antibodies: rabbit anti-glial fibrillary acidic protein (GFAP) (Dako, Glostrup, Denmark, #ZO334, 1:500), rabbit anti-ionized calcium-binding adaptor molecule 1 (IBA1) (Wako, #PDF3116, 1:5000), and rabbit anti-calbindin CD28K (Invitrogen, #PAS-85669, 1:500) in blocking buffer at 4 °C overnight. The sections were then washed in washing buffer (blocking buffer diluted 1:50 in PBBS) and incubated for one hour with biotinylated goat anti-rabbit IgG (Vector, #BA-1000)

Table 1
Sample size, genotype, age, and sex of the mice included in the study.

Number of mice	Genotype	Age	Sex
5	NPC2−/−	6 weeks	2 females 3 males
5	NPC2+/+	6 weeks	3 females 2 males
6	NPC2−/−	12 weeks	2 females 4 males
6	NPC2+/+	12 weeks	3 females 3 males

diluted 1:200 in blocking buffer. To visualize antibody binding, the sections were incubated with Avidin-Biotin complex system (ABC-HRP kit, Vector, #PK6100) and 3,3′-diaminobenzidine tetrahydrochloride (DAB). All sections were mounted with Pertex.

PFA-fixed visceral tissue (liver, lungs, and spleen) designated for histopathological analysis was dehydrated in increasing ethanol concentrations (70 %, 96 %, and 100 %), followed by clearing in a xylene substitute before being embedded in paraffin. The tissue blocks were cut into three μm sections on a microtome (Leica RM2255, Germany) and placed on Superfrost Plus glass slides. Tissue samples were rehydrated and stained with Mayer's Hematoxylin (MHS 16, Sigma-Aldrich) and Eosin Y (HT110116, Sigma-Aldrich) solution.

The sections were imaged with an Axioplan 2 microscope equipped with an Axiocam MRc camera (Carl Zeiss). Images were analyzed with ImageJ software (Schindelin et al., 2012) and adjusted for contrast and brightness.

2.6. Statistical analysis

All data analysis was done in GraphPad Prism version 9.4.1. *P*-values ≤0.05 were considered significant. Data were tested for normality and equal variance by the D'Agostino-Pearson and F-test, respectively. Due to low n-values in some datasets, only the F-test was applied in such circumstances. If the dataset passed these tests, a *t*-test was used to compare the two groups. If data did not pass, non-parametric analysis was performed. For statistical evaluation of the deviation from the expected mendelian frequency, a chi-square test was performed. The exact statistical test and sample size are described in the figure legends. Results are presented with mean ± standard deviation (SD) unless stated otherwise.

3. Results

3.1. Breeding outcome

Breeding data were collected from continuous trio breeding of heterozygous *Npc2*+/− mice for a 10-week study period. The mating resulted in offspring either homozygous for the wild-type alleles (*Npc2*+/+), heterozygotes (*Npc2*+/−), or homozygous for the gene trap alleles (*Npc2*−/−). The genotype ratio was 27 %:58.5 %:14.5 %, respectively, from 200 offspring. Only one out of seven offspring was born with the *Npc2*−/− genotype, which deviated significantly ($p = 0.0024$) from the expected ratio of an autosomal recessive disease (25 %:50 %:25 %), suggesting increased embryo-fetal death due to NPC2 deficiency.

All breeding cages gave birth to at least one litter, and 60 % of the breeding cages gave birth to five or more litters during the 10-week study period. 21 days after birth, all remaining offspring (93.6 %) were robust and ready to be weaned. A few mice died before the time of weaning due to cannibalism, and 2 % of the offspring were stillborn. The stillborn mice were excluded from the litter size at birth (Table 2).

3.2. Phenotype

At six weeks of age, *Npc2*+/+ and *Npc2*−/− mice were indistinguishable concerning their phenotype (Fig. S2 and supplemental video material). They were comparable in body size (Fig. 1A+B), and no symptoms were visible. However, even though not present with any symptoms, *Npc2*−/− mice exhibited splenomegaly already at six weeks of age (Fig. 1D). Although not significant, the lungs were also enlarged compared to WT littermates (*Npc2*+/+: 0.17 ± 0.07 g, *Npc2*−/−: 0.24 ± 0.08 g). The weight of the liver and brain was comparable between WT and NPC2-deficient mice at this age. All *Npc2*−/− mice developed tremors from about eight weeks of age (Supplemental video material), which increased in severity until the time of euthanasia. As the tremor progressed, the motor function declined. This was evident during observations of their movement and rearing activity. The gait was wobbly, with the feet pointing away from the body ("duck feet"), and mild hindlimb splay was present during rearing. With increasing age, ataxia gait followed (Fig. S2). At the end stage of the disease, the rearing behavior was reduced, and when attempting to rear, they often lost their balance (Supplemental video material). At 12 weeks, *Npc2*−/− mice weighed less than WT controls ($p = 0.002$) (Fig. 1C). From six to 12 weeks of age, *Npc2*+/+ mice increased their body weight by 34.9 % (Fig. 1A-C). Oppositely hereto, the body weight of female *Npc2*−/− mice stagnated, whereas male *Npc2*−/− mice lost weight from 10 weeks of age (data not shown). All *Npc2*−/− mice were euthanized at 12 weeks of age due to reaching one of the humane endpoints; weighing 20 % less compared to WT mice of identical age and sex (Fig. 1A+C).

When looking at the affected organs in the NP-C2 mouse model at 12 weeks of age (Fig. 1E), the brain was weighing 11.0 % less in *Npc2*−/− mice compared to the WT control mice. In contrast, the lungs and spleen were enlarged by 59.8 % and 31.1 %, respectively, compared to the respective organs in the *Npc2*+/+ mice. Accordingly, the NP-C2 mouse model is characterized by growth retardation, brain atrophy, splenomegaly, and possible pulmonary involvement.

Table 2
The breeding outcome after trio matings for a 10-week study period.

Interlitter interval (days)[a]	26 ± 7.2
No. of litters per trio	4.75 ± 2.3
Litter size at birth	6.23 ± 2.41
Litter size at weaning	5.83 ± 2.55
% loss at weaning (mortality)	6.4 %
Weight at weaning (g)	12.01 ± 1.77

[a] Number of days between births of consecutive litters.

3.3. Brain pathology

3.3.1. Purkinje cell degeneration

One of the hallmarks of NP-C is severe loss of cerebellar Purkinje cells (PCs), which is evident in both patients and animal models of NP-C (Markmann et al., 2018; Sarna et al., 2003; Li et al., 2005; Chandler et al., 2017; Elrick et al., 2010). Therefore, a thorough examination of the PC degeneration in the *Npc2*−/− mouse model was performed using the PC marker Calbindin-D28k (Whitney et al., 2008).

When looking at the cerebellum from WT mice independent of age, the morphology appeared normal with both a homogenous PC layer and molecular layer whereto the PC dendrites extended. At six weeks of age, *Npc2*−/− mice exhibited a varying degree of PC degeneration (Fig. 2). The PC loss resulted in a striated appearance in the PC layer, which was especially evident in the anterior lobe, including both the hemispheric region and the vermis (Fig. 2B+C). The PC loss was more pronounced in the anterior lobe compared to the posterior (data not shown). However, some areas of the cerebellum were still completely unaffected. Furthermore, pathological changes in the morphology of the PCs were apparent, with focal axonal swellings and storage material seen in the soma of some PCs even at this early stage of the disease (Fig. 2H+I).

From six to 12 weeks of age, severe progressive PC degeneration occurred, although the loss of the PCs still varies regionally throughout the cerebellum (Fig. 3). The hemispheric regions, as well as the anterior part of the vermal region, were especially affected, showing an almost complete loss of PCs with only a few cells scattered around in this particular area (Figs. 3-4). In opposite hereto, the PCs remained almost unaffected in the flocculus, lobules IX and X of the cerebellar vermis, although some degree of PC degeneration was initiated in the lobule IX resulting in a striated appearance (Fig. 3F). This pattern of PC loss was evident in all of the 12-week-old NPC2-deficient mice.

At 12 weeks of age, more pronounced axonal swelling was seen in the remaining PCs (Fig. 4), possibly due to the more advanced accumulation of storage material at the end stage of the disease (Sarna et al., 2003). Axonal swellings were almost identified in all surviving PCs.

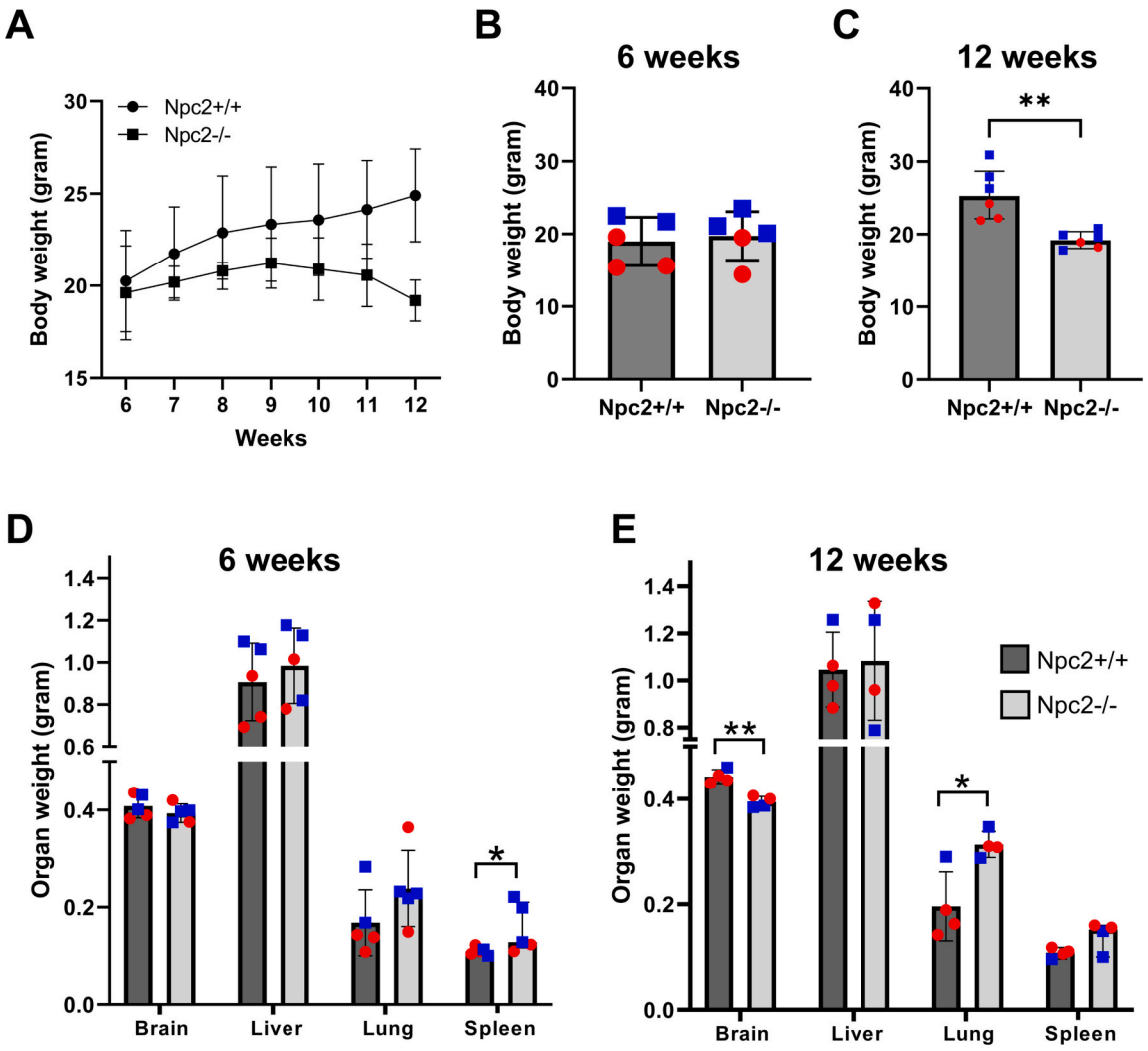

Fig. 1. Body- and organ weight in the wild-type (*Npc2*+/+) and NPC2 deficient (*Npc2*−/−) mice at 6 and 12 weeks of age. A) Body weight over time. *Npc2*−/− has a lower increase in body weight from six to nine weeks of age compared to *Npc2*+/+ mice, after which the body weight of *Npc2*−/− mice declines until 12 weeks of age, where the NPC2-deficient mice reach one of the humane endpoints; weighing 20 % less than age-matched wild-type mice of the same sex. (*Npc2*+/+: $n = 6$–11 mice, *Npc2*−/−: $n = 3$–8 mice). Mean ± SD. B) No difference is seen in body weight at six weeks of age when comparing the *Npc2*−/− mice with age-matched *Npc2*+/+ ($n = 5$ mice/group). Two-tailed *t*-test, (t[8] = 0.360, $p = 0.728$). Mean ± SD. C) At 12 weeks, the body weight of *Npc2*−/− mice is significantly lower compared to *Npc2*+/+ mice (n = 6 mice/group). Mann-Whitney *U* test (U = 0, n1 = n2 = 5, $^{**}p = 0.0022$). Median with interquartile range. D) At six weeks of age *Npc2*−/− mice have significantly larger spleens than *Npc2*+/+ controls. Data were analyzed with the Mann-Whitney U test (U = 2.5, n1 = n2 = 5, $^{*}p = 0.04$, two-tailed) due to a significant difference in the F-test ($p = 0.005$). Median with interquartile range. No differences are seen in the weight of the brain (t[8] = 1.065, $p = 0.318$), liver (t[8] = 0.674, $p = 0.519$), and lung (t[8] = 1.520, $p = 0.167$) when comparing the two groups analyzed with a two-tailed t-test (n = 5 mice/group). Mean ± SD. E) At the end-stage of the disease, the weight of the brains is significantly lower in *Npc2*−/− mice compared with *Npc2*+/+ controls (t[6] = 5.799, $^{**}p = 0.001$), whereas the lungs are significantly larger (t[6] = 3.349, $^{*}p = 0.015$). There are no differences in organ weight of the liver (t[6] = 0.251, $p = 0.810$) and spleen (t[6] = 2.281, $p = 0.0627$) at this time point ($n = 4$ mice/group). The data were analyzed with a two-tailed t-test. Mean ± SD. Blue squares: males, red circles: females.

Furthermore, changes in the dendritic arborization were evident in some of the PCs, e.g., sprouting of the dendrites in the mediolateral plane (Fig. 4C). Even though the preservation of PCs was seen in the nodulus (lobule X), widespread axonal swellings were also visualized in the granular layer of the nodulus (Fig. 4I) indicating that the surviving PCs were affected by the NPC2 deficiency. Thus, the abnormalities seen in the PCs progressed from six to 12 weeks of age, where severe and widespread morphological changes were evident.

3.3.2. *Neuroinflammation*

Neuroinflammation in different brain regions, including the cerebral cortex, striatum, hippocampus, thalamus, cerebellum, and medulla oblongata, was evaluated immunohistochemically using the astrocyte and microglia cell markers GFAP and IBA1, respectively. Both astrocytes and microglia contribute to the disease progression in NP-C (Lopez et al., 2011; Baudry et al., 2003; Cougnoux et al., 2018), and thus a thorough examination of these cell types at six and 12 weeks of age was performed.

In WT mice of both six and 12 weeks of age, only a few GFAP-positive cells were seen in the brain, except in the hippocampus, where astrocytes were abundantly present (Figs. 5 and 7). The astrocytes were often found adjacent to blood vessels, and they exhibited a typical astrocytic morphology with small somata and fine branching processes. At six weeks of age, three out of five NPC2-deficient mice already exhibited pronounced astrogliosis (two males and one female) (Fig. 5C), whereas the other two *Npc2*−/− mice (one male and one female) were indistinguishable from WT littermates. When analyzing the aforementioned brain regions in the affected 6-week-old *Npc2*−/− mice, widespread

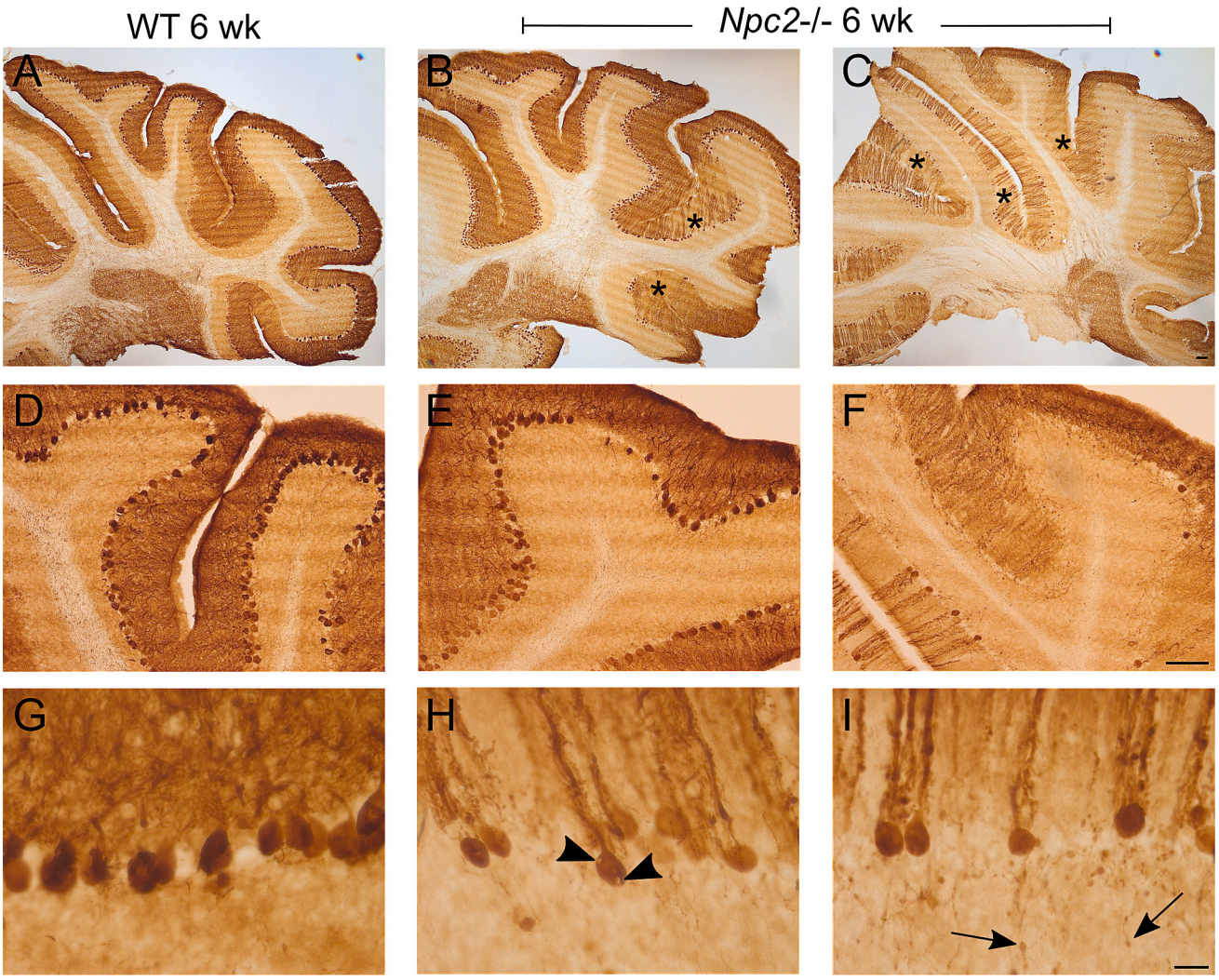

Fig. 2. Cerebellar Purkinje cell degeneration in six weeks old *Npc2*−/− mice. The cerebellum sections were evaluated immunohistochemically with the cerebellar Purkinje cell marker calbindin. Cerebellar Purkinje cell degeneration is already present at six weeks of age giving the molecular layer a striated appearance, see asterisks for examples. Furthermore, accumulation of storage material can be seen in the cerebellar Purkinje cells (arrowhead) as well as focal axonal swelling (arrows) in the cerebellum of *Npc2*−/− mice. The degeneration of Purkinje neurons varies among the *Npc2*−/− mice; thus, two different scenarios are included in this figure. The images are representative of wild-type (WT) control (n = 3 mice) and *Npc2*−/− (n = 5 mice). Scale bar = 100 μm (A-F), and 20 μm (G-I).

astrogliosis was present, especially in the cerebral cortex, hippocampus, and cerebellum. Reactive astrocytes were particularly localized at the PC layer of the cerebellum. In some cerebellar regions, the distribution and morphology of the astrocytes remained unchanged (Fig. 5I).

When looking at microglia in six weeks old mice, an increase in the number, as well as a change in morphology, was evident in all *Npc2*−/− mice, although to a varying degree (Fig. 6). Reactive microglia, indicated by retracted and thickened processes, were found scattered in different regions of the cerebrum with a particularly high occurrence in the hippocampus. The most pronounced microglial reaction was, however, seen in the cerebellum. Resting ramified microglia were still present in all *Npc2*−/− mice. As for the astrocytes, the reactive microglia were primarily located at the PC layer. In the most severely affected mice (three out of five), reactive microglia were also present in the molecular layer (Fig. 6L+O). Besides the processes' thickening, the microglia's somata were swollen compared to the microglia of WT mice. Widespread microgliosis was also seen in the deep cerebellar nuclei.

The inflammatory areas of the cerebellum probably corresponded to the regions with PC degeneration. Thus, more severe microgliosis was found in the *Npc2*−/− mice with pronounced astrogliosis and PC degeneration. At six weeks of age, before symptom development, mild PC loss and varying degrees of neuroinflammation are already present.

When analyzing the aforementioned brain regions in 12-week-old mice, apparent differences in the expression of GFAP between *Npc2*−/− and WT mice were evident (Fig. 7). In the *Npc2*−/− mice, many reactive astrocytes were found in all brain regions examined indicating severe diffuse astrogliosis. In addition, the cellular appearance of the astrocytes changed further when compared to that of the six-week-old mice, now showing pronounced hypertrophy of somata and extended processes. Due to the increased number of astrocytes, astrocytic processes overlap, resulting in a blurred appearance, especially in the thalamus and cerebellum, making it difficult to identify the individual astrocytes.

As for the astrocytes, the number of IBA1 immunopositive cells was also markedly increased in all brain regions at 12 weeks of age (Fig. 7). Additionally, the reactive microglia were severely enlarged, resulting in an amoeboid appearance, indicating an active phagocytic state (Colombo et al., 2021). This was particularly evident in the cerebellum, where reactive microglial cells were abundantly found in both the molecular and the granular layers. In WT mice, the microglia were only lightly stained, sparse in number, and exhibited a normal morphology with small somata and few processes.

The widespread PC loss, astrogliosis, and activated microglia indicated progressive neurodegeneration and neuroinflammation at the end-

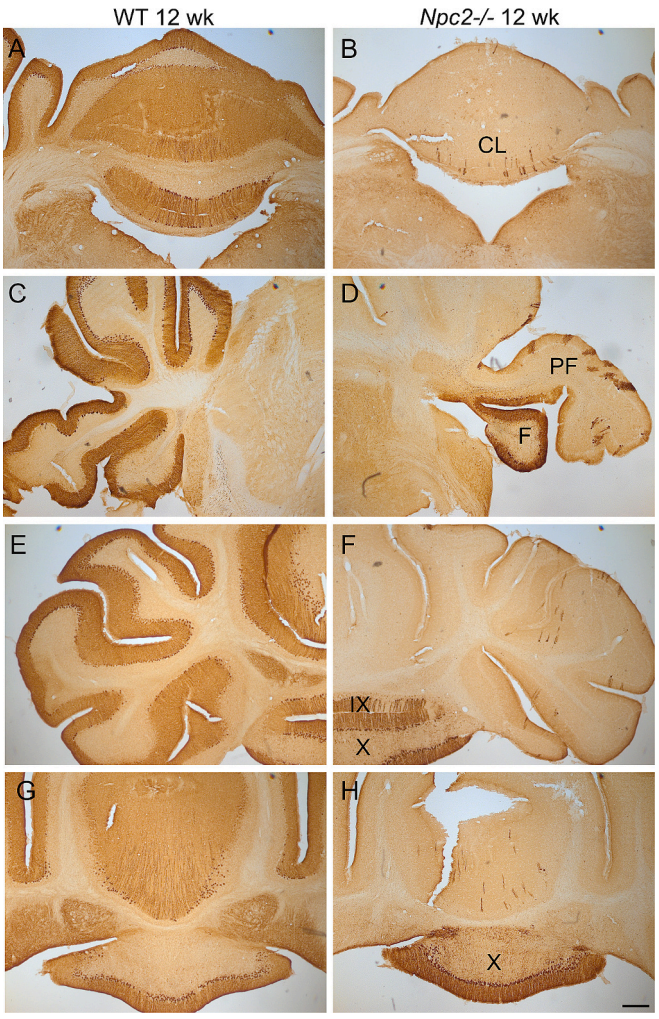

Fig. 3. Cerebellar Purkinje cell degeneration in 12-weeks-old *Npc2−/−* mice. Normal cerebellar Purkinje cell patterns are seen in wild-type (WT) mice (A, C, E, G) compared to *Npc2−/−* mice (B, D, F, H). The loss of Purkinje neurons is more pronounced in the anterior cerebellar vermis (B) compared to the lobules located more posterior, where preservation of Purkinje neurons is seen in the flocculus (D), lobules IX and X (F, H). Almost complete loss of cerebellar Purkinje cells is seen in the cerebellar hemisphere (F). The sections are stained with the cerebellar Purkinje cell marker calbindin. The images are representative of $n = 3$ mice/group. CL = central lobule of vermis, PF = paraflocculus, F = flocculus, IX = the ninth lobule of vermis, X = nodulus. Scale bar = 300 μm.

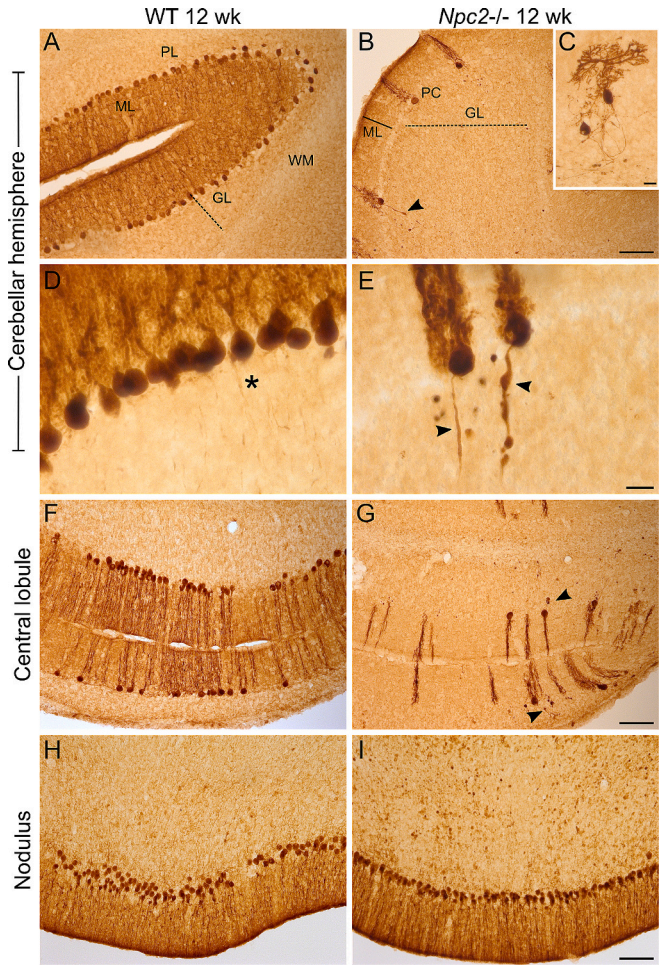

Fig. 4. Cerebellar Purkinje cell pathology in 12-weeks-old *Npc2−/−* mice. Cerebellar sections are evaluated immunohistochemically using the Purkinje neuron marker calbindin. Only a few remaining cerebellar Purkinje cells are seen in the hemispheric region of *Npc2−/−* mice (B, C, E) compared to wild-type (WT) mice (A, D). The morphology of the surviving Purkinje neurons reveals severe pathology. Some Purkinje neurons show increased dendritic branching in the mediolateral plane (C). Whereas thin axons (asterisk) appear in the WT mice (D), axonal swellings (arrowhead) are seen in the granular layer in *Npc2−/−* mice. The cerebellar Purkinje cell degeneration follows a specific pattern and the anterior vermis, e.g., the central lobule (G), has an extensive loss, whereas the Purkinje neurons in the lobule X (nodulus) are preserved (I). Numerous axonal swellings are still present in the granular layer of the nodulus (I). GL = granular layer, PL = Purkinje cell layer, ML = molecular layer, PC = cerebellar Purkinje cells, WM = white matter. The images are representative of n = 3 mice/group. Scale bar = 100 μm (A, B, F, G, H, I), 20 μm (C, D, E).

stage of NP-C2. These pathological findings are associated with the severe disease phenotype characterized by tremor and ataxia gait seen 12 weeks old *Npc2−/−* mice.

3.4. Visceral pathology

The histopathology of the liver, spleen, and lungs was evaluated in the *Npc2−/−* mice at six and 12 weeks of age using hematoxylin and eosin staining and compared to WT control mice.

At six weeks of age none or mild pathological findings were seen in the visceral organs of *Npc2−/−* mice characterized by the accumulation of a few foamy macrophages and focal inflammation (Fig. 8). At this time point, hypertrophy and hyperplasia of Kupffer cells were observed in the liver, which eventually will progress to foam cells. The pathological findings were most obvious in the spleen, corresponding to the splenomegaly observed at six weeks of age. However, the degree of pathology varied among the different *Npc2−/−* mice (data not shown).

When evaluating the lungs of the NPC2-deficient mice, it appeared consolidated, evident even at low magnification (data not shown). The alveolar space was filled with eosinophilic proteinaceous material, which was more evident at higher magnification (Fig. 9). This could indicate the presence of alveolar proteinosis. At higher magnification, large clusters of foamy macrophages were present intra-alveolar and in the alveolar air space. Lipid-laden vesicles were evident in the cytoplasm of these macrophages (Fig. 9). Furthermore, the intra-alveolar septae were thickened with increased cellularity as a result of pulmonary inflammatory response. This thickening resulted in an increased diffusion barrier compared to control animals.

The pathology observed in the liver of 12 weeks old *Npc2−/−* mice varied among the different mice assessed, ranging from mild to severe affection of the liver tissue (Fig. S3A). The main pathological findings for all mice assessed were large numbers of foamy macrophages found in clusters within the sinusoids (Fig. 9). The pathological changes were

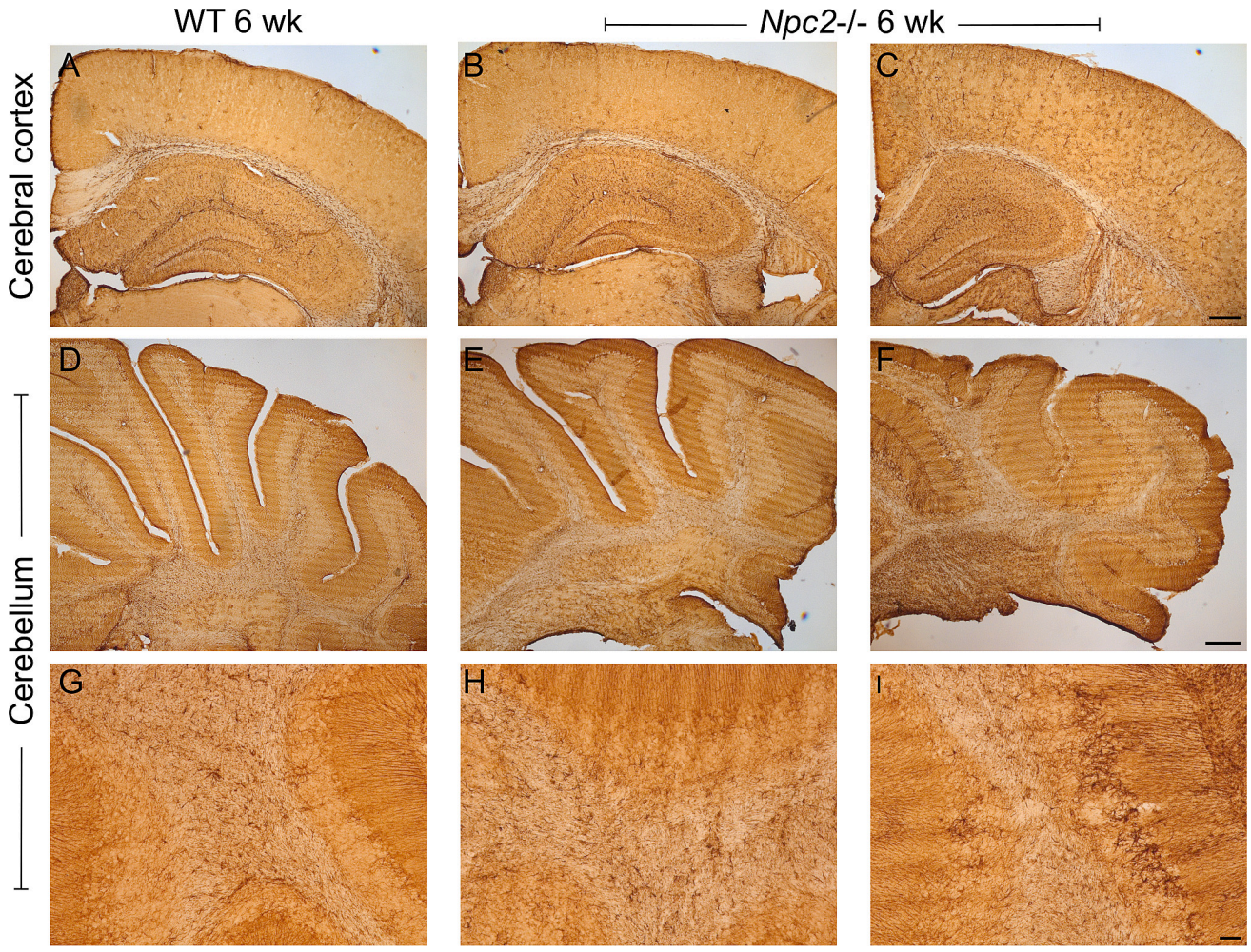

Fig. 5. GFAP immunohistochemistry in 6-weeks-old *Npc2*−/− and wild-type (WT) control littermates. GFAP-positive astrocytes are sparse in the brain of wild-type (WT) mice (A, D, G). There is a large variation in the *Npc2*−/− group with two out of five *Npc2*−/− mice (B, E, H) being indistinguishable from the WT mice. In three out of five *Npc2*−/− mice (C, F, I), widespread astrogliosis is already apparent in, e.g., the cerebral cortex and hippocampus. Furthermore, reactive astrocytes are also found in some areas of the cerebellum, often associated with the Purkinje cell layer (I). Two examples for each region are included to demonstrate the variation found between the *Npc2*−/− mice. Three WT and five *Npc2*−/− mice were analyzed for GFAP immunoreactivity. Scale bar = 300 μm (A-F), 50 μm (G-I).

widespread but often centered around the central veins of the liver. In the most severely affected mice, only a few areas with normal hepatic architecture remained in periportal areas surrounding the portal vein, which could be observed even at low magnification.

Foam cells are known to induce inflammation, and inflammatory foci could be seen with lymphocytes, monocytes, and neutrophils present in several regions of the liver. Furthermore, hemorrhage and focal necrosis with karyolysis were also evident in the diseased liver (Fig. S3B).

Similar to the pathological findings in the liver, a widespread accumulation of foam cells was present in the spleen of *Npc2*−/− mice resulting in a disorganization of the normal histoanatomical architecture, making it difficult to distinguish white pulp regions (Fig. 9). These histopathological findings correlated well with the splenomegaly seen in the *Npc2*−/− mice. In opposite hereto, the spleens from WT mice were well-organized with clear boundaries between the red and white pulp with an apparent marginal zone. Extramedullary hematopoiesis is a common finding in the splenic red pulp of healthy mice (Suttie, 2006), and in accordance, megakaryocytes were also present in the tissue of WT mice (Fig. 9).

4. Discussion

This study reports on a thorough histopathological characterization of the *Npc2*$^{Gt(LST105)BygNya}$ mouse model performed at two different ages i.e., before the onset of symptoms and at the end stage of the disease. The pathology of the brain and visceral organs was investigated to evaluate the translatability of this NPC2-deficient murine model to NP-C patients, with a particular focus on disease progression and neuropathology.

4.1. Breeding of *Npc2*−/− mice

NPC2 deficiency ultimately led to infertility in both sexes, which necessitated breeding with heterozygotes (Busso et al., 2010; Busso et al., 2014). NPC2 is required to produce functionally mature spermatozoa, probably involved in inducing capacitation (Busso et al., 2014), and in female mice, loss of a functional NPC2 causes defects in steroidogenesis in the ovaries due to inadequate cholesterol transport (Busso et al., 2010). The number of homozygous *Npc2*−/− mice born was expected to be every fourth due to the autosomal recessive inheritance pattern (Vanier, 2010). However, only a single out of seven mice had the desired *Npc2*−/− genotype, suggesting embryonic lethality (Sleat et al., 2004). These findings are in line with previously described

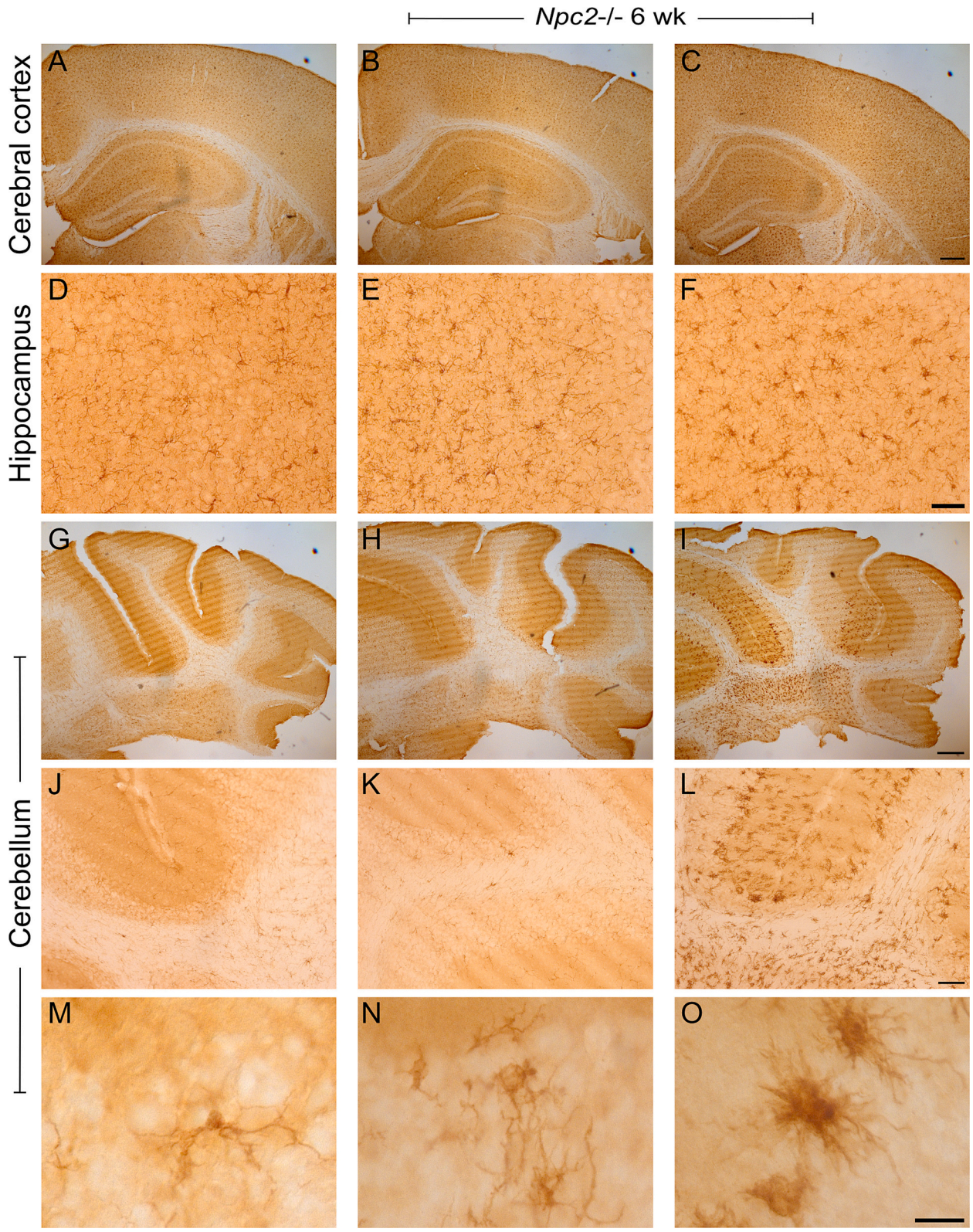

Fig. 6. IBA1 immunohistochemistry in 6-weeks-old *Npc2−/−* and wild-type (WT) control littermates. The pattern of microglia activation was evaluated in different regions of the brain: cerebral cortex (A-C), hippocampus (D—F), and cerebellum (G-O). Prominent microgliosis is present in the cerebellum of diseased mice. However, the morphology of the reactive microglia varies among the different *Npc2−/−* mice. In WT mice, the microglia are characterized by a small soma with ramified processes (M). In *Npc2−/−* mice, the microglia transform into an active state with enlargement of the soma and thickening of processes (N), with the most prominent changes seen in (O) where the microglia are characterized by an amoeboid shape indicative of phagocytotic state. Three WT and five *Npc2−/−* mice were analyzed. Scale bar = 300 μm (A-C, G-I), 50 μm (D—F), and 20 μm (J-L, M-O).

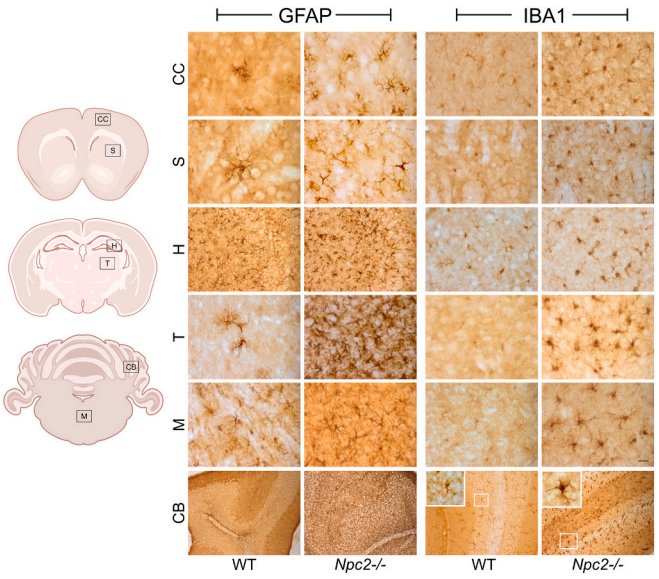

Fig. 7. Neuroinflammation in the *Npc2*−/− mice at 12 weeks of age. Astrogliosis and reactive microglia are evident throughout the entire brain of *Npc2*−/− mice compared to age-matched wild-type (WT) controls. CC = cerebral cortex, S = striatum, H = hippocampus, T = thalamus, M = medulla oblongata, CB = cerebellum. Images are representative of n = 3 mice/group. Scale bar = 20 μm and 50 μm (CB).Created with Biorender.com.

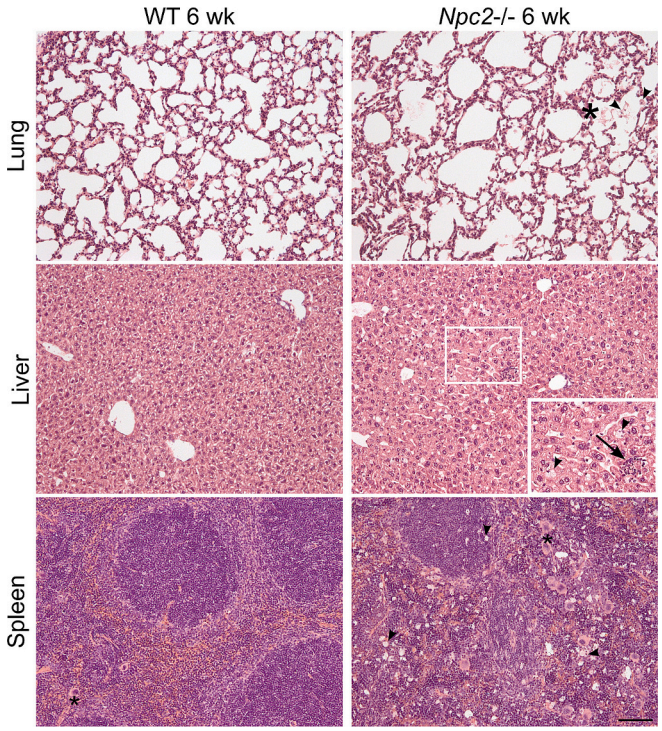

Fig. 8. Visceral histopathology in six weeks old *Npc2*−/− mice evaluated using hematoxylin and eosin staining. Normal histological organization of the lung, liver, and spleen was seen in wild-type (WT) mice. Mild pathological findings are seen in the visceral organs of *Npc2*−/− mice at six weeks of age. In the lungs, either none or only a very few foam cells (arrowheads) and sparse eosinophilic material (large asterisk) are observed in the alveolar lumen. Similarly, an accumulation of storage material is found within the Kupffer cells in the sinusoids of the liver (arrowheads). Foci with inflammatory cells (arrow) are observed in the liver (highlighted in the white box). The most prominent findings are seen in the spleen with a more widespread observation of foam cells (arrowheads). The megakaryocytes (small asterisks) are increased in the spleen of *Npc2*−/− mice probably as a response to the foam cell accumulation. Scale bar = 100 μm.

findings for this NP-C2 mouse model and other NP-C murine models (Sleat et al., 2004; Morris et al., 1982). Two percent of the offspring were stillborn, however, the risk of perinatal cannibalism could result in an underestimation of the number of stillborns. Patient cases with the severe neonatal onset form of NP-C resulting in stillbirth have previously been described (Imrie et al., 2015; Spiegel et al., 2009). Unfortunately, the stillborn mice were not genotyped, and whether these pups were *Npc2*−/−is unknown. When working with genetically modified mouse strains where only a few pups are born with the desired genotype, several aspects of the breeding program need attention. The trio breeding used in the present study is a good strategy for rapid colony expansion, and when using continuous breeding, this approach possibly reduces the inter-litter interval by taking advantage of post-partum estrus (Chatkupt et al., 2018). Cross-fostering results in more robust offspring (Heiderstadt et al., 2014; Heiderstadt and Blizard, 2011), which was supported here by a mean weaning weight of 12.01 ± 1.77 g. Higher mortality from birth to weaning was seen in our study compared to healthy BALB/cJ (#000651) (Flurkey et al., 2009).

4.2. Genotype

The *Npc2*−/− mouse model is established using the gene trap approach to introduce an insertional mutation in the genome of 129P2/OlaHsd mouse embryonic stem cells. The gene trap vector is located in the intron immediately downstream of the first exon. Subsequently, the gene trap insertion results in a fusion protein including the first 27 amino acids of the NPC2 protein, which are encoded by exon1 of the *Npc2* gene (Nielsen et al., 2011). Although the gene trap mutation is expected to produce a null allele type, one disadvantage of the gene trap approach is that alternative splicing can result in low levels of the WT protein (Lee et al., 2007). Consequently, the $Npc2^{Gt(LST105)BygNya}$ mouse model is hypomorph. Based on this knowledge, with none or only low expression of normal NPC2, this correlates well with the fast disease progression seen in the *Npc2*−/− mouse model in the present study. This reflects the human situation where the severity of the mutation (e.g., frameshift, nonsense, or missense) correlates with the clinical phenotype (e.g., the onset of symptoms, progression, and age of death) (Millat et al., 2001; Verot et al., 2007; Chikh et al., 2005; Geberhiwot et al., 2018).

4.3. Phenotype

Weight loss is a common finding in mouse models of NP-C2 (Nielsen et al., 2011; Sleat et al., 2004; Markmann et al., 2018), why this was also expected in these *Npc2*−/− mice holding the gene-trap mutation, rederived from the mouse strain used by Nielsen et al., where progressive weight loss from 70 days of age and until termination at 12 weeks of age has previously been reported (Nielsen et al., 2011). To our surprise, only the male *Npc2*−/− mice lost weight during the 12-week study period, whereas only growth retardation was evident in female *Npc2*−/− mice (data not shown). Health status is an important variable in animal studies, which consequently can affect the results (Van Keuren and Saunders, 2004). The NPC2-deficient mouse strain was rederived to specific pathogen-free facilities different from the study performed by Nielsen and colleagues (Nielsen et al., 2011). Recent years' research has revealed a clear significance of the gut microbiota on the brain and the immune system (Hickman et al., 2018; Minter et al., 2016; Sampson et al., 2016). Hindlimb clasping and penile prolapse were previously observed in these mice maintained on a BALB/c background at 12 weeks of age (Rasmussen et al. unpublished data), which was not the case after the rederivation. None of the *Npc2*−/− mice in the present study developed hindlimb clasping or penile prolapse (Fig. S2C). These symptoms are both markers of disease progression, indicating severe impairment of the cerebellum, including its efferent and afferent projections (Markmann et al., 2018; Yerger et al., 2022; Fu et al., 2012). Discrepancies in health status and gut microbiota are possible

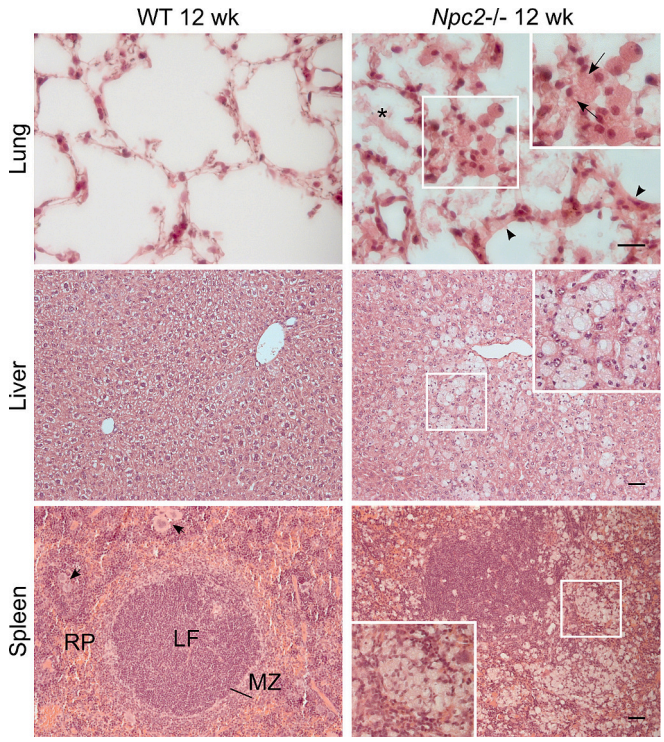

Fig. 9. Visceral histopathology in 12 weeks old *Npc2−/−* mice. Normal histological organization of the lung, liver, and splenic tissue is evident in wild-type (WT) mice compared to *Npc2−/−* mice.The main pathological finding in the visceral organs examined from *Npc2−/−* mice is a severe accumulation of foam cells. The white boxes identify the accumulation of foamy macrophages. Lipid inclusions are evident intracellularly in the lung macrophages (arrows). The histopathology of the lung tissue is characterized by thickening of the alveolar wall (arrowheads) and focal intra-alveolar accumulation of eosinophilic granular material suggestive of proteinosis (asterisk). Small arrows point to megakaryocytes indicating extramedullary hematopoiesis in the spleen. The white pulp consists of LF = lymphoid follicle and MZ = marginal zone (black line), RP = red pulp. Representative tissue sections from WT and *Npc2−/−* (n = 3 mice/group) stained with hematoxylin and eosin. Scale bar = 20 μm (lung), 50 μm (liver and spleen).

explanations for the difference between the *Npc2−/−* mice used in the present study and those used previously (Nielsen et al., 2011). However, this is not studied further.

Only a few studies are available on *Npc2−/−* mice, and hardly any on the *Npc2−/−* mice holding the LST105 mutation (Nielsen et al., 2011; Schrantz et al., 2007). There is, therefore, a clear need for a thorough characterization of this NP-C2 mutant mouse, important for future work with the specific disease model.

When comparing the NP-C2 mouse model of the present study ($Npc2^{Gt(LST105)BygNya}$) with the NPC2-deficient murine model induced by gene targeting ($Npc2^{tm1Plob}$), differences prevail (Sleat et al., 2004; Markmann et al., 2018). Hence, the disease phenotype in the $Npc2^{tm1Plob}$ mice is less progressive, with the mice reaching disease end-stage at 14 or 16 weeks of age depending on sex (Markmann et al., 2018), which is clearly later compared to the 12 weeks seen in the $Npc2^{Gt(LST105)BygNya}$ mouse used in the present study. Strain background could have a significant effect on survival, which has also been described for the $Npc2^{tm1Plob}$ mouse strain (Dixit et al., 2011; Sleat et al., 2004). However, both murine models are retained on a BALB/c background and are hypomorphic, but the approach for establishing the genetically modified mouse models differed, as mentioned previously. In patients, the type of genetic mutation is associated with the disease phenotype (Verot et al., 2007; Chikh et al., 2005). Thus this could be an explanation for the variation seen in these two mouse models of NP-C2. For a comparison between the two NP-C2 mouse models, see supplemental Table 1.

4.4. Brain pathology

NP-C2 is a progressive neurodegenerative disorder, which is the primary cause of mortality (Ramirez et al., 2014). The major pathological hallmark of NP-C2 is cholesterol accumulation in the lysosomes of all cells due to impaired lipid transport. The most prominent increase in cholesterol levels is observed in the visceral organs (Nielsen et al., 2011; Li et al., 2005; Xie et al., 2000; Te Vruchte et al., 2004). However, increased brain cholesterol levels in the $Npc2^{Gt(LST105)BygNya}$ mouse model have also been observed compared to WT mice (Nielsen et al., 2011). In the previous study by Nielsen et al., total cholesterol levels in different brain regions of the *Npc2−/−* mice were quantified, and they found a significant increase in cholesterol levels, especially in the cerebellum, and to a lesser extent in the cerebral cortex of *Npc2−/−* mice. In contrast, the cholesterol levels of the hippocampus were comparable between WT and *Npc2−/−* mice (Nielsen et al., 2011). This correlates well with the fact that the cerebellum is more vulnerable to NPC2 deficiency compared to other brain regions, although the underlying reason is unknown (Elrick et al., 2010). Consequently, another hallmark of NP-C2 is severe PC loss, which progresses in an age-dependent manner resulting in cerebellar atrophy (Sarna et al., 2003; German et al., 2001; Walterfang et al., 2013; Gilbert et al., 1981). Similar to observations of human NP-C2 and other mouse models of NP-C2 (German et al., 2001; Walterfang et al., 2013; Jahnova et al., 2014; Bjurulf et al., 2008), neurodegeneration leads to brain atrophy in *Npc2−/−* mice of the current study.

Additional morphological changes in PCs are lipid storage and axonal swellings. These pathological hallmarks were previously described in other mouse models of NPC (Sleat et al., 2004; Sarna et al., 2003; Baudry et al., 2003; Zervas et al., 2001; Dominko et al., 2021). Axonal swellings, also called torpedoes, precede neuronal death and are associated with axon dysfunction in neurodegenerative disorders like Alzheimer's disease, amyotrophic lateral sclerosis, and other demyelinating disorders (Mejia Maza et al., 2019; Lang-Ouellette et al., 2021; Takahashi et al., 1997; Stokin et al., 2005; Louis et al., 2009; Redondo et al., 2015). Axonal swellings are very conspicuous in early-onset human NP-C and increase in number with disease progression (Walkley and Suzuki, 2004). At six weeks of age, mild axonal swellings are evident in *Npc2−/−* mice. As the disease progresses, more storage material accumulates correlating well with the severe axonal swellings observed in the remaining Purkinje neurons in 12 weeks-old *Npc2−/−* mice (Bjurulf et al., *2008;* Zervas et al., *2001;* Elleder et al., *1985*).

The anterior-to-posterior PC loss in the *Npc2−/−* mice was similarly reported elsewhere (Sarna et al., 2003; Higashi et al., 1993; Ko et al., 2005). The differences in cell death among the PCs, and especially the delayed degeneration of the PC in the nodulus have been extensively studied, e.g., with a focus on a possible correlation between cholesterol accumulation and vulnerability. However, the difference in the neuronal capability of cholesterol storage is not an explanation for this variation, as cholesterol storage is also noted in the PCs of the nodulus (Ko et al., 2005). Despite this, the progression of PC death correlates well with the development of symptoms attributable to cerebellar pathology. Thus, the *Npc2−/−* mice of the present study are relevant for further investigation of this gradual degeneration of the cerebellar nodules, important for increasing the understanding of the pathological processes leading to PC death.

In the explanation of PC death, necroptosis (Cougnoux et al., 2016), autophagy (Ko et al., 2005; Liao et al., 2007), oxidative stress (Vázquez et al., 2011), and neuroinflammation (Baudry et al., 2003; Kavetsky et al., 2019) were suggested as major causes. It was strongly indicated that neuroinflammation actively participates in the disease progression, and neuroinflammation is also a pathological hallmark in human NP-C2 patients (Cachón-González et al., 2018; Cologna et al., 2014; Peake et al., 2011). In the present study, neuroinflammation was observed in both six and 12 weeks old *Npc2−/−* mice and progressed severely with age, hence correlating to the progression of PC death. The pattern of

neuroinflammation varied among the youngest mice, but at six weeks of age, microgliosis was already evident in the cerebellum of all NPC2-deficient mice. In contrast, astrogliosis was only present in 60 % of the *Npc2−/−* mice, indicating that microgliosis precedes astrogliosis, which correlated with a previous study on neuroinflammation in NP-C mice (Baudry et al., 2003).

Microglia are present at an early stage of NP-C1 even when PC loss is absent (Baudry et al., 2003; Kavetsky et al., 2019). It remains unknown why and how early reactive microglia can be observed in this NP-C2 mouse model. In 40 % of the six weeks old *Npc2−/−* mice, only mild morphological changes were observed among the microglia with most of the microglia cells having a resting phenotype similar to that of microglia in the WT mice; i.e., thin cell bodies with ramified processes (Baudry et al., 2003), indicating that neuroinflammation is in its waking stage. Severe progression in neuroinflammation then follows from six to 12 weeks of age, terminating with significant loss of PCs accompanied by widespread astrogliosis and reactive microglia. At the end stage of the disease, all areas of the cerebellum are affected, and the inflammatory cells were not only located at the border of the PC layer, as seen in the early stage of the disease. The inflammation had further progressed to the entire brain.

The variability in the degree of neuroinflammation and PC degeneration at six weeks of age challenges the treatment of NP-C2 even further, especially since the symptoms first develop weeks later. From a therapeutic perspective, the gradual increase in neuroinflammation and PC degeneration from six weeks and onwards implies a need for early intervention, which is difficult since the disease is rarely diagnosed until after the onset of neurological symptoms (Imrie et al., 2015; Patterson et al., 2020). As little as 5 % of the normal number of PCs is sufficient to retain normal motor function (Elleder et al., 1985; Peake et al., 2011). However, irreversible neurodegeneration hinders successful treatment of the disease (Imrie et al., 2015; Verot et al., 2007; Patterson et al., 2020).

4.5. Visceral pathology

The symptoms related to NP-C are heterogeneous, making the diagnosis challenging for physicians (Imrie and Wraith, 2001). Splenomegaly denotes a major sign of systemic involvement and is present in approximately 85 % of patient cases (Vanier, 2010). In the *Npc2−/−* mouse, splenomegaly was present at six weeks of age, hence before the onset of symptoms, which is comparable with the juvenile form of human NP-C, where isolated splenomegaly can be the debuting sign of disease denoting a possible relevance for early disease identification (Vanier, 2010; Verot et al., 2007; Jahnova et al., 2014; Imrie and Wraith, 2001). Splenomegaly frequently precedes the onset of neurological symptoms, which also were the case in the *Npc2−/−* mice. Two weeks before symptom development, the spleen was severely enlarged with a weight increase of approximately 40 % compared to WT mice. Splenomegaly can regress with age (Vanier, 2010), but this was not the case in the NPC2-deficient mice. At 12 weeks of age, splenomegaly persisted with severe infiltration of foamy macrophages in the splenic tissue of all *Npc2−/−* mice assessed.

NPC2 deficiency also results in the disposition of excess cholesterol in the liver, and hepatomegaly is a common clinical finding in patients suffering from NP-C (Sleat et al., 2004). Despite a thorough histopathological examination of the liver of the NP-C2 mice, hepatomegaly was not detected at six or 12 weeks, but using hematoxylin and eosin staining histopathological findings consistently showed foamy Kupffer cells, a hallmark of the disease, in the sinusoids. In NP-C2 patients, the accumulation of lipid storage is often more pronounced in the spleen than in the liver, where deposits range from almost undetectable to widespread intracellular storage resulting in liver impairment (Vanier, 2010; Jahnova et al., 2014; Elleder et al., 1984; Sheth et al., 2017).

The lung is another organ severely affected in NP-C2 patients, and some patients are dying from respiratory failure (Verot et al., 2007; Sheth et al., 2017; Griese et al., 2010). In six-week-old *Npc2−/−* mice, enlarged lungs were also evident, although not significantly. However, at 12 weeks of age, all NPC2-deficient mice had pulmonary abnormalities characterized by the accumulation of foamy macrophages, thickened alveolar septae, and eosinophilic proteinacous material in the alveolar lumen. In addition, the severe lung infiltration caused an increased weight of the lung tissue in *Npc2−/−* mice; findings comparable with those seen in human patients, where, e.g., lung biopsies reveal accumulation of eosinophilic protein-rich material indicative of proteinosis and foamy macrophages (Verot et al., 2007; Bjurulf et al., 2008; Sheth et al., 2017; Griese et al., 2010).

The accumulation of foamy macrophages in all non-cerebral organs examined denotes a common pathological finding in NP-C patients (Lopez et al., 2012) and the specific NP-C2 mouse model examined here. Loss of NPC2 results in dysfunction of the intracellular cholesterol transport in all cells of the body and subsequently affects their normal function. The balance between influx and efflux of low-density lipoproteins becomes disturbed, consequently converting macrophages into foamy macrophages, the typical phenotype observed in NP-C (Russell et al., 2009; van Eijk and Aerts, 2021). Normally, an increase in macrophages is seen as a response to inflammation. However, foamy macrophages further escalate the inflammation by presenting with a pro-inflammatory phenotype (Russell et al., 2009) via the secretion of pro-inflammatory cytokines, thereby contributing to the exacerbation of disease progression (Cougnoux et al., 2018).

When using mice as models for human diseases, it is important to be aware of the differences between mice and humans. One of the most important things to consider in regard to NP-C2 is differences in lipoprotein metabolism. Humans have high plasma levels of low-density lipoprotein (LDL)-cholesterol. In opposite hereto, most of the cholesterol in mice is transported in high-density lipoprotein (HDL) particles (Oppi et al., 2019; Sontag et al., 2013). Cellular uptake of cholesterol is normally via the LDL-receptor pathway, where LDL becomes hydrolyzed to cholesterol (Hede et al., 2021; Xie et al., 1999). As a consequence, mice have an overall lower level of cholesterol when compared to humans (Oppi et al., 2019).

5. Conclusion

The *Npc2−/−* mice develop a neurovisceral pathology similar to NP-C2 in humans. The mouse model resembles the juvenile form of human NP-C2 with splenomegaly as the only manifestation weeks before the onset of neurological symptoms, which mainly relates to the pathology of the cerebellum (Sheth et al., 2017; Devaraj et al., 2022; Synofzik et al., 2016). Pathological changes are evident early in the brain, with mild PC degeneration and neuroinflammation where reactive microglia predominate. The disease in *Npc2−/−* mice severely progressed from six to 12 weeks of age with pronounced cholesterol accumulation and widespread neurodegeneration correlating with clinical symptoms. At the end-stage of the disease, *Npc2−/−* mice are characterized by tremor, ataxia gait, growth retardation, severe PC degeneration, brain atrophy, widespread neuroinflammation, and severe cholesterol storage in the liver, lungs, and spleen. The *Npc2−/−* mice present a genotype-phenotype correlation as that seen in humans emphasizing the translational value of this NP-C2 mouse model. The $Npc2^{Gt(LST105)BygNya}$ mice will be valuable for further assessment of disease progression and for testing of new treatment strategies.

CRediT authorship contribution statement

Charlotte Laurfelt Munch Rasmussen: Conceptualization, Investigation, Methodology, Writing – original draft, Writing – review & editing, Funding acquisition. **Louiza Bohn Thomsen:** Conceptualization, Writing – review & editing. **Christian Würtz Heegaard:** Conceptualization, Methodology, Writing – review & editing. **Torben Moos:** Conceptualization, Writing – review & editing, Funding acquisition.

Annette Burkhart: Conceptualization, Writing – review & editing, Funding acquisition.

Declaration of competing interest

The authors declare that they have no known competing financial interests or personal relationships that could have appeared to influence the work reported in this paper.

Data availability

Data will be made available on request.

Acknowledgements

We would like to thank laboratory technicians Merete Fredsgaard and Hanne Krone Nielsen, Aalborg University, Denmark, and animal technician Karina Holm Lassen, Aarhus University, Denmark, for their excellent technical assistance.

Funding support

This work was kindly supported by Fonden til Lægevidenskabens Fremme, Torben og Alice Frimodts Fond, Hørslev-Fonden, Læge Sophus Carl Emil Friis og Hustru Olga Doris Friis Legat, Direktør Emil C. Hertz og hustru Inger Hertz' Fond, Dagmar Marshalls Fond, and Research Initiative on Blood-Brain Barriers and Drug Delivery founded by the Lundbeck Foundation (Grant no. 2013-14113).

Appendix A. Supplementary data

Supplementary data to this article can be found online at https://doi.org/10.1016/j.mcn.2023.103880.

References

Baudry, M., Yao, Y., Simmons, D., Liu, J., Bi, X., 2003. Postnatal development of inflammation in a murine model of Niemann–Pick type C disease: immunohistochemical observations of microglia and astroglia. Exp. Neurol. 184 (2), 887–903.

Berzina, Z., Solanko, L.M., Mehadi, A.S., Jensen, M.L.V., Lund, F.W., Modzel, M., et al., 2018. Niemann-Pick C2 protein regulates sterol transport between plasma membrane and late endosomes in human fibroblasts. Chem. Phys. Lipids 213, 48–61.

Bjurulf, B., Spetalen, S., Erichsen, A., Vanier, M.T., Strøm, E.H., Strømme, P., 2008. Niemann-Pick disease type C2 presenting as fatal pulmonary alveolar lipoproteinosis: morphological findings in lung and nervous tissue. Med. Sci. Monit. 14 (8).

Busso, D., Oñate-Alvarado, M.J., Balboa, E., Zanlungo, S., Moreno, R.D., 2010. Female infertility due to anovulation and defective steroidogenesis in NPC2 deficient mice. Mol. Cell. Endocrinol. 315 (1–2), 299–307.

Busso, D., Oñate-Alvarado, M.J., Balboa, E., Castro, J., Lizama, C., Morales, G., et al., 2014. Spermatozoa from mice deficient in Niemann-Pick disease type C2 (NPC2) protein have defective cholesterol content and reduced in vitro fertilising ability. Reprod. Fertil. Dev. 26 (4), 609–621.

Cachón-González, M.B., Zaccariotto, E., Cox, T.M., 2018. Genetics and therapies for GM2 gangliosidosis. Curr. Gene Ther. 18 (2), 68–89.

Chandler, R.J., Williams, I.M., Gibson, A.L., Davidson, C.D., Incao, A.A., Hubbard, B.T., et al., 2017. Systemic AAV9 gene therapy improves the lifespan of mice with Niemann-Pick disease, type C1. Hum. Mol. Genet. 26 (1), 52–64.

Chatkupt, T.T., Libal, N.L., Mader, S.L., Murphy, S.J., Saunders, K.E., 2018. Effect of continuous trio breeding compared with continuous pair breeding in 'shoebox' caging on measures of reproductive performance in estrogen receptor knockout mice. J. Am. Assoc. Lab. Anim. Sci. 57 (4), 328.

Chikh, K., Rodriguez, C., Vey, S., Vanier, M.T., Millat, G., 2005. Niemann-Pick type C disease: subcellular location and functional characterization of NPC2 proteins with naturally occurring missense mutations. Hum. Mutat. 26 (1), 20–28.

Cologna, S.M., Cluzeau, C.V.M., Yanjanin, N.M., Blank, P.S., Dail, M.K., Siebel, S., et al., 2014. Human and mouse neuroinflammation markers in Niemann-Pick disease, type C1. J. Inherit. Metab. Dis. 37 (1), 83–92.

Colombo, A., Dinkel, L., Müller, S.A., Sebastian Monasor, L., Schifferer, M., Cantuti-Castelvetri, L., et al., 2021. Loss of NPC1 enhances phagocytic uptake and impairs lipid trafficking in microglia. Nat. Commun. 12, 1158.

Cougnoux, A., Cluzeau, C., Mitra, S., Li, R., Williams, I., Burkert, K., et al., 2016. Necroptosis in Niemann–Pick disease, type C1: a potential therapeutic target. Cell Death Dis. 7 (3), e2147.

Cougnoux, A., Drummond, R.A., Collar, A.L., Iben, J.R., Salman, A., Westgarth, H., et al., 2018. Microglia activation in Niemann-Pick disease, type C1 is amendable to therapeutic intervention. Hum. Mol. Genet. 27 (12), 2076–2089.

Devaraj, R., Mahale, R.R., Sindhu, D.M., Stezin, A., Kamble, N., Holla, V.V., et al., 2022. Spectrum of movement disorders in Niemann-Pick disease type C. In: Tremor and Other Hyperkinetic Movements, 12(1).

Dixit, S.S., Jadot, M., Sohar, I., Sleat, D.E., Stock, A.M., Lobel, P., 2011. Loss of Niemann-Pick C1 or C2 protein results in similar biochemical changes suggesting that these proteins function in a common lysosomal pathway. PLoS One 6 (8), 23677.

Dominko, K., Rastija, A., Sobocanec, S., Vidatic, L., Meglaj, S., Babic, A.L., et al., 2021. Impaired retromer function in Niemann-Pick type C disease is dependent on intracellular cholesterol accumulation. Int. J. Mol. Sci. 22 (24), 13256.

van Eijk, M., Aerts, J.M.F.G., 2021. The unique phenotype of lipid-laden macrophages. Int. J. Mol. Sci. 22 (8).

Elleder, M., Smíd, F., Hyniová, H., Čihula, J., Zeman, J., Macek, M., 1984. Liver findings in Niemann-Pick disease type C. Histochem. J. 16, 1147–1170.

Elleder, M., Jirásek, A., Šmíd, F., Ledvinová, J., Besley, G.T.N., 1985. Niemann-Pick disease type C. Acta Neuropathol. 66 (4), 325–336.

Elrick, M.J., Pacheco, C.D., Yu, T., Dadgar, N., Shakkottai, V.G., Ware, C., et al., 2010. Conditional Niemann-Pick C mice demonstrate cell autonomous Purkinje cell neurodegeneration. Hum. Mol. Genet. 19 (5), 837.

Flurkey, K., Currer, J.M., Leiter, E.H., Witham, B. (Eds.), 2009. The Jackson Laboratory Handbook on Genetically Standardized Mice, 6th ed. The Jackson Laboratory, Bar Harbor, pp. 1–396.

Fu, H., Bartz, J.D., Stephens, R.L., McCarty, D.M., 2012. Peripheral nervous system neuropathology and progressive sensory impairments in a mouse model of mucopolysaccharidosis IIIB. PLoS One 7 (9), e45992.

Geberhiwot, T., Moro, A., Dardis, A., Ramaswami, U., Sirrs, S., Marfa, M.P., et al., 2018. Consensus clinical management guidelines for Niemann-Pick disease type C. Orphanet J. Rare Dis. 13 (1), 50.

German, D.C., Matthew Quintero, E., Liang, C.L., Ng, B., Punia, S., Xie, C., et al., 2001. Selective neurodegeneration, without neurofibrillary tangles, in a mouse model of Niemann-Pick C disease. J. Comp. Neurol. 433 (3), 415.

Gilbert, E.F., Callahan, J., Viseskul, C., Opitz, J.M., 1981. Niemann-Pick disease type C. Eur. J. Pediatr. 136 (3), 263–274.

Griese, M., Brasch, F., Aldana, V.R., Cabrera, M.M., Goelnitz, U., Ikonen, E., et al., 2010. Respiratory disease in Niemann-Pick type C2 is caused by pulmonary alveolar proteinosis. Clin. Genet. 77 (2), 119–130.

Hede, E., Christiansen, C.B., Heegaard, C.W., Moos, T., Burkhart, A., 2021. Gene therapy to the blood-brain barrier with resulting protein secretion as a strategy for treatment of Niemann Picks type C2 disease. J. Neurochem. 156 (3), 290–308.

Heiderstadt, K.M., Blizard, D.A., 2011. Increased juvenile and adult body weights in BALB/cByJ mice reared in a communal nest. J. Am. Assoc. Lab. Anim. Sci. 50 (4), 484.

Heiderstadt, K.M., Vandenbergh, D.J., Gyekis, J.P., Blizard, D.A., 2014. Communal nesting increases pup growth but has limited effects on adult behavior and neurophysiology in inbred mice. J. Am. Assoc. Lab. Anim. Sci. 53 (2), 152.

Hickman, S., Izzy, S., Sen, P., Morsett, L., El Khoury, J., 2018. Microglia in neurodegeneration. Nat. Neurosci. 21 (10), 1359–1369.

Higashi, Y., Murayama, S., Pentchev, P.G., Suzuki, K., 1993. Cerebellar degeneration in the Niemann-Pick type C mouse. Acta Neuropathol. 85 (2), 175–184.

Imrie, J., Wraith, J.E., 2001. Isolated splenomegaly as the presenting feature of Niemann–Pick disease type C. Arch. Dis. Child. 84 (5), 427–429.

Imrie, J., Heptinstall, L., Knight, S., Strong, K., 2015. Observational cohort study of the natural history of Niemann-Pick disease type C in the UK: a 5-year update from the UK clinical database. BMC Neurol. 15, 257.

Jahnova, H., Dvorakova, L., Vlaskova, H., Hulkova, H., Poupetova, H., Hrebicek, M., et al., 2014. Observational, retrospective study of a large cohort of patients with Niemann-Pick disease type C in the Czech Republic: a surprisingly stable diagnostic rate spanning almost 40 years. Orphanet J. Rare Dis. 9, 140.

Kavetsky, L., Green, K.K., Boyle, B.R., Yousufzai, F.A.K., Padron, Z.M., Melli, S.E., et al., 2019. Increased interactions and engulfment of dendrites by microglia precede Purkinje cell degeneration in a mouse model of Niemann Pick type-C. Sci. Rep. 9 (1), 14722.

Ko, D.C., Milenkovic, L., Beier, S.M., Manuel, H., Buchanan, J.A., Scott, M.P., 2005. Cell-autonomous death of cerebellar Purkinje neurons with autophagy in Niemann-Pick type C disease. PLoS Genet. 1 (1), 81–95.

Lang-Ouellette, D., Gruver, K.M., Smith-Dijak, A., Blot, F.G.C., Stewart, C.A., de Vanssay de Blavous, P., et al., 2021. Purkinje cell axonal swellings enhance action potential fidelity and cerebellar function. Nat. Commun. 12 (1), 1–13.

Lee, T., Shah, C., Xu, E.Y., 2007. Gene trap mutagenesis: a functional genomics approach towards reproductive research. Mol. Hum. Reprod. 13 (11), 771–779.

Li, H., Repa, J.J., Valasek, M.A., Beltroy, E.P., Turley, S.D., German, D.C., et al., 2005. Molecular, anatomical, and biochemical events associated with neurodegeneration in mice with Niemann-Pick type C disease. J. Neuropathol. Exp. Neurol. 64 (4), 323–333.

Li, X., Saha, P., Lib, J., Blobel, G., Pfeffer, S.R., 2016. Clues to the mechanism of cholesterol transfer from the structure of NPC1 middle lumenal domain bound to NPC2. Proc. Natl. Acad. Sci. U. S. A. 113 (36), 10079–10084.

Liao, G., Yao, Y., Liu, J., Yu, Z., Cheung, S., Xie, A., et al., 2007. Cholesterol accumulation is associated with lysosomal dysfunction and autophagic stress in Npc1 −/− mouse brain. Am. J. Pathol. 171 (3).

Liu, B., Li, H., Repa, J.J., Turley, S.D., Dietschy, J.M., Liu, B., et al., 2008. Genetic variations and treatments that affect the lifespan of the NPC1 mouse. J. Lipid Res. 49 (3), 663–669.

Loftus, S.K., Morris, J.A., Carstea, E.D., Gu, J.Z., Cummings, C., Brown, A., et al., 1997. Murine model of Niemann-Pick C disease: Mutation in a cholesterol homeostasis gene. Science (80-) 277 (5323), 232–235.
Lopez, M.E., Klein, A.D., Dimbil, U.J., Scott, M.P., 2011. Anatomically Defined Neuron-Based Rescue of Neurodegenerative Niemann–Pick Type C Disorder. J. Neurosci. 31 (12), 4367–4378.
Lopez, M.E., Klein, A.D., Hong, J., Dimbil, U.J., Scott, M.P., 2012. Neuronal and epithelial cell rescue resolves chronic systemic inflammation in the lipid storage disorder Niemann-Pick C. Hum. Mol. Genet. 1;21(13), 2946–2960.
Louis, E.D., Faust, P.L., Vonsattel, J.P.G., Honig, L.S., Rajput, A., Rajput, A., et al., 2009. Torpedoes in Parkinson's disease, Alzheimer's disease, essential tremor, and control brains. Mov. Disord. 24 (11), 1600–1605.
Markmann, S., Christie-Reid J, J., Rosenberg, J.B., De BP, Kaminsky S.M., Crystal, R.G., et al., 2018. Attenuation of the Niemann-Pick type C2 disease phenotype by intracisternal administration of an AAVrh.10 vector expressing Npc2. Exp. Neurol. 306, 22–33.
Mejia Maza, A., Carmen-Orozco, R.P., Carter, E.S., Dávila-Villacorta, D.G., Castillo, G., Morales, J.D., et al., 2019. Axonal swellings and spheroids: a new insight into the pathology of neurocysticercosis. Brain Pathol. 29 (3), 425–436.
Millat, G., Chikh, K., Naureckiene, S., Sleat, D.E., Fensom, A.H., Higaki, K., et al., 2001. Niemann-Pick disease type C: spectrum of HE1 mutations and genotype/phenotype correlations in the NPC2 group. Am. J. Hum. Genet. 69 (5), 1013–1021.
Minter, M.R., Zhang, C., Leone, V., Ringus, D.L., Zhang, X., Oyler-Castrillo, P., et al., 2016. Antibiotic-induced perturbations in gut microbial diversity influences neuro-inflammation and amyloidosis in a murine model of Alzheimer's disease. Sci. Rep. 6, 30028.
Morris, M.D., Bhuvaneswaran, C., Shio, H., Fowler, S., 1982. Lysosome lipid storage disorder in NCTR-BALB/c mice. I. Description of the disease and genetics. Am. J. Pathol. 108 (2), 140–149.
Nielsen, G.K., Dagnaes-Hansen, F., Holm, I.E., Meaney, S., Symula, D., Andersen, N.T., et al., 2011. Protein replacement therapy partially corrects the cholesterol-storage phenotype in a mouse model of Niemann-Pick type C2 disease. PLoS One 6 (11), e27287.
Ong, W.Y., Sundaram, R.K., Huang, E., Ghoshal, S., Kumar, U., Pentchev, P.G., et al., 2004. Neuronal localization and association of Niemann pick C2 protein (HE1/NPC2) with the postsynaptic density. Neuroscience. 128 (3), 561–570.
Oppi, S., Lüscher, T.F., Stein, S., 2019. Mouse models for atherosclerosis research — which is my line? Front. Cardiovasc. Med. 6, 46.
Patterson, M.C., Garver, W.S., Giugliani, R., Imrie, J., Jahnova, H., Meaney, F.J., et al., 2020. Long-term survival outcomes of patients with Niemann-Pick disease type C receiving miglustat treatment: a large retrospective observational study. J. Inherit. Metab. Dis. 43 (5), 1060–1069.
Peake, K.B., Campenot, R.B., Vance, D.E., Vance, J.E., 2011. Niemann-Pick type C1 deficiency in microglia does not cause neuron death in vitro. Biochim. Biophys. Acta 1812 (9), 1121–1129.
Ramirez, C.M., Lopez, A.M., Le, L.Q., Posey, K.S., Weinberg, A.G., Turley, S.D., 2014. Ontogenic changes in lung cholesterol metabolism, lipid content, and histology in mice with Niemann–Pick type C disease. Biochim. Biophys. Acta 1841 (1), 54–61.
Redondo, J., Kemp, K., Hares, K., Rice, C., Scolding, N., Wilkins, A., 2015. Purkinje cell pathology and loss in multiple sclerosis cerebellum. Brain Pathol. 25 (6), 692–700.
Roszell, B.R., Tao, J.-Q., Yu, K.J., Gao, L., Huang, S., 2013. Pulmonary abnormalities in animal models due to Niemann-Pick type C1 (NPC1) or C2 (NPC2) disease. PLoS One 8 (7), 67084.
Russell, D.G., Cardona, P.J., Kim, M.J., Allain, S., Altare, F., 2009. Foamy macrophages and the progression of the human tuberculosis granuloma. Nat. Immunol. 10 (9), 943–948.
Sampson, T.R., Debelius, J.W., Thron, T., Janssen, S., Shastri, G.G., Ilhan, Z.E., et al., 2016. Gut microbiota regulate motor deficits and neuroinflammation in a model of Parkinson's disease. Cell. 167 (6), 1469–1480.
Sarna, J.R., Larouche, M., Marzban, H., Sillitoe, R.V., Rancourt, D.E., Hawkes, R., 2003. Patterned Purkinje cell degeneration in mouse models of Niemann-Pick type C disease. J. Comp. Neurol. 456 (3), 279–291.
Schindelin, J., Arganda-Carreras, I., Frise, E., Kaynig, V., Longair, M., Pietzsch, T., et al., 2012. Fiji: an open-source platform for biological-image analysis. Nat. Methods 9, 676–682.
Schrantz, N., Sagiv, Y., Liu, Y., Savage, P.B., Bendelac, A., Teyton, L., 2007. The Niemann-Pick type C2 protein loads isoglobotrihexosylceramide onto CD1d molecules and contributes to the thymic selection of NKT cells. J. Exp. Med. 204 (4), 841.
Sheth, J., Joseph, J.J., Shah, K., Muranjan, M., Mistri, M., Sheth, F., 2017. Pulmonary manifestations in Niemann-Pick type C disease with mutations in NPC2 gene: case report and review of literature. BMC Med. Genet. 18, 5.
Sleat, D.E., Wiseman, J.A., El-Banna, M., Price, S.M., Verot, L., Shen, M.M., et al., 2004. Genetic evidence for nonredundant functional cooperativity between NPC1 and NPC2 in lipid transport. Proc. Natl. Acad. Sci. U. S. A. 101 (16), 5886–5891.
Sontag, T.J., Chellan, B., Getz, G.S., Reardon, C.A., 2013. Differing rates of cholesterol absorption among inbred mouse strains yield differing levels of HDL-cholesterol. J. Lipid Res. 54 (9), 2515–2524.
Spiegel, R., Raas-Rothschild, A., Reish, O., Regev, M., Meiner, V., Bargal, R., et al., 2009. The clinical spectrum of fetal Niemann-Pick type C. Am. J. Med. Genet. Part A. 149A (3), 446–450.
Stokin, G.B., Lillo, C., Falzone, T.L., Brusch, R.G., Rockenstein, E., Mount, S.L., et al., 2005. Axonopathy and transport deficits early in the pathogenesis of Alzheimer's disease. Science (80-) 307 (5713), 1282–1288.
Suttie, A.W., 2006. Histopathology of the spleen. Toxicol. Pathol. 34, 466–503.
Synofzik, M., Fleszar, Z., Schöls, L., Just, J., Bauer, P., Torres Martin, J.V., et al., 2016. Identifying Niemann–Pick type C in early-onset ataxia: two quick clinical screening tools. J. Neurol. 263 (10), 1911–1918.
Takahashi, T., Yagishita, S., Amano, N., Yamaoka, K., Kamei, T., 1997. Amyotrophic lateral sclerosis with numerous axonal spheroids in the corticospinal tract and massive degeneration of the cortex. Acta Neuropathol. 94 (3), 294–299.
Te Vruchte, D., Lloyd-Evans, E., Veldman, R.J., Neville, D.C.A., Dwek, R.A., Platt, F.M., et al., 2004. Accumulation of glycosphingolipids in Niemann-Pick C disease disrupts endosomal transport. J. Biol. Chem. 279 (25), 26167–26175.
Van Keuren, M.L., Saunders, T.L., 2004. Rederivation of transgenic and gene-targeted mice by embryo transfer. Transgenic Res. 13 (4), 363–371.
Vanier, M.T., 2010. Niemann-Pick disease type C. Orphanet J. Rare Dis. 5, 16.
Vázquez, M.C., del Pozo, T., Robledo, F.A., Carrasco, G., Pavez, L., Olivares, F., et al., 2011. Alteration of gene expression profile in Niemann-Pick type C mice correlates with tissue damage and oxidative stress. PLoS One 6 (12), e28777.
Verot, L., Chikh, K., Freydière, E., Honoré, R., Vanier, M.T., Millat, G., 2007. Niemann–Pick C disease: functional characterization of three NPC2 mutations and clinical and molecular update on patients with NPC2. Clin. Genet. 71 (4), 320–330.
Walkley, S.U., Suzuki, K., 2004. Consequences of NPC1 and NPC2 loss of function in mammalian neurons. Biochim. Biophys. Acta 1685 (1–3), 48–62.
Walterfang, M., Patenaude, B., Abel, L.A., Kluenemann, H., Bowman, E.A., Fahey, M.C., et al., 2013. Subcortical volumetric reductions in adult Niemann-Pick disease type C: a cross-sectional study. Am. J. Neuroradiol. 34 (7), 1334–1340.
Whitney, E.R., Kemper, T.L., Rosene, D.L., Bauman, M.L., Blatt, G.J., 2008. Calbindin-D28k is a more reliable marker of human Purkinje cells than standard Nissl stains: a stereological experiment. J. Neurosci. Methods 168 (1), 42–47.
Wiweger, M., Majewski, L., Adamek-Urbanska, D., Wasilewska, I., Kuznicki, J., 2021. npc2-deficient zebrafish reproduce neurological and inflammatory symptoms of Niemann-Pick type C disease. Front. Cell. Neurosci. 15.
Xie, C., Turley, S.D., Dietschy, J.M., 1999. Cholesterol accumulation in tissues of the Niemann-Pick type C mouse is determined by the rate of lipoprotein-cholesterol uptake through the coated-pit pathway in each organ. Proc. Natl. Acad. Sci. U. S. A. 96 (21), 11992–11997.
Xie, C., Burns, D.K., Turley, S.D., Dietschy, J.M., 2000. Cholesterol is sequestered in the brains of mice with Niemann-Pick type C disease but turnover is increased. J. Neuropathol. Exp. Neurol. 59 (12), 1106–1117.
Yañez, M.J., Marín, T., Balboa, E., Klein, A.D., Alvarez, A.R., Zanlungo, S., 2020. Finding pathogenic commonalities between Niemann-Pick type C and other lysosomal storage disorders: opportunities for shared therapeutic interventions. Biochim. Biophys. Acta Mol. Basis Dis. 1866 (10), 165875.
Yerger, J., Cougnoux, A.C., Abbott, C.B., Luke, R., Clark, T.S., Cawley, N.X., et al., 2022. Phenotype assessment for neurodegenerative murine models with ataxia and application to Niemann-Pick disease, type C1. Biol. Open. 11 (4), bio059052.
Zervas, M., Dobrenis, K., Walkley, S.U., 2001. Neurons in Niemann-Pick disease type C accumulate gangliosides as well as unesterified cholesterol and undergo dendritic and axonal alterations. J. Neuropathol. Exp. Neurol. 60 (1), 49–64.
Zhou, S., Davidson, C., Mcglynn, R., Stephney, G., Dobrenis, K., Vanier, M.T., et al., 2011. Endosomal/lysosomal processing of gangliosides affects neuronal cholesterol sequestration in Niemann-Pick disease type C. Am. J. Pathol. 179 (2), 890–902.